Cancer Science
Japanese Cancer Association JCA
Open Access

In vivo subcellular imaging of tumors in mouse models using a fluorophore-conjugated anti-carcinoembryonic antigen antibody in two-photon excitation microscopy

Shigehiro Koga,[1,2,3] Yusuke Oshima,[1,3,4,5] Naoki Honkura,[1,3,6] Tadahiro Iimura,[3,4,5] Kenji Kameda,[7] Koichi Sato,[2] Motohira Yoshida,[2] Yuji Yamamoto,[2] Yuji Watanabe,[2] Atsuhiko Hikita[1,3,4] and Takeshi Imamura[1,3,4,5]

Departments of [1]Molecular Medicine for Pathogenesis ; [2]Gastrointestinal Surgery and Surgical Oncology, Ehime University Graduate School of Medicine, Ehime; [3]Core Research for Evolutional Science and Technology, Japan Science and Technology Agency, Ehime; [4]Division of Bio-imaging, Proteo-Science Center, Ehime University, Ehime; [5]Translational Research Center, Ehime University Hospital, Ehime, Japan; [6]Department of Immunology, Genetics and Pathology, Rudbeck Laboratory, Uppsala University, Uppsala, Sweden; [7]Integrated Center for Science Shigenobu Station, Ehime University, Ehime, Japan

Key words

Cancer cells, carcinoembryonic antigen, fluorophore-conjugated antibodies, *in vivo* fluorescence imaging, two-photon excitation microscopy

Correspondence

Takeshi Imamura and Atsuhiko Hikita, Department of Molecular Medicine for Pathogenesis, Ehime University Graduate School of Medicine, Ehime, Shitsukawa, Toon, Ehime 791-0295, Japan.
Tel: +81-89-960-5044; Fax: +81-89-960-5052;
E-mails: timamura-ind@umin.ac.jp and ahikita-tky@umin.ac.jp

Funding Information

This study was supported by MEXT KAKENHI Grant Number 22113004, and JSPS KAKENHI Grant Number 23390368, 26670667, 24680060. T.I. was supported by Naito Foundation and Takeda Foundation.

Received June 10, 2014; Revised August 3, 2014; Accepted August 4, 2014

Cancer Sci **105** (2014) 1299–1306

doi: 10.1111/cas.12500

Recently, there has been growing interest in applying fluorescence imaging techniques to the study of various disease processes and complex biological phenomena *in vivo*. To apply these methods to clinical settings, several groups have developed protocols for fluorescence imaging using antibodies against tumor markers conjugated to fluorescent substances. Although these probes have been useful in macroscopic imaging, the specificity and sensitivity of these methods must be improved to enable them to detect micro-lesions in the early phases of cancer, resulting in better treatment outcomes. To establish a sensitive and highly specific imaging method, we used a fluorophore-conjugated anti-carcinoembryonic antigen (CEA) antibody to perform macroscopic and microscopic *in vivo* imaging of inoculated cancer cells expressing GFP with or without CEA. Macroscopic imaging by fluorescence zoom microscopy revealed that bio-conjugation of Alexa Fluor 594 to the anti-CEA antibody allowed visualization of tumor mass consisting of CEA-expressing human cancer cells, but the background levels were unacceptably high. In contrast, microscopic imaging using a two-photon excitation microscope and the same fluorescent antibody resulted in subcellular-resolution imaging that was more specific and sensitive than conventional imaging using a fluorescence zoom microscope. These results suggest that two-photon excitation microscopy in conjunction with fluorophore-conjugated antibodies could be widely adapted to detection of cancer-specific cell-surface molecules, both in cancer research and in clinical applications.

The survival rates of cancer patients have increased dramatically over the past a few decades, due to both improvements in treatments and advances in diagnostic methods. In particular, early detection of cancer lesions is key to more favorable prognoses. For example, today almost all patients with colorectal carcinoma *in situ* survive beyond 5 years. However, cancer is still a major cause of death, and metastases and recurrences of cancer are critical issues in treatment.[1] Detection of small lesions in the resection edges and target organs of metastases, such as lymph nodes, may have positive effects on treatment outcomes.

Bio-imaging techniques have become indispensable tools in both biological studies and clinical diagnosis. In recent years, computed tomography, positron emission tomography, single-photon emission computed tomography and MRI have become popular and indispensable methods that are routinely used in clinical practice and for evaluation of therapeutic efficacy.[2–4] Although these techniques excel in penetration depth, their resolution and specificity are not sufficient to detect micro-lesions, such as cancer *in situ* or very early phases of lymph-node metastasis. Fluorescence imaging provides a method for detection of specific molecules at subcellular resolution that is potentially superior to conventional imaging modalities; however, it has not been extensively applied in clinical settings, in part because of limitations on penetration depth and excessive background signals.[2–4]

Fluorophore-conjugated antibodies against various targets, including growth factor receptors, have been used for the detection of several kinds of cancers in mouse models. Using these reagents, epidermal growth factor receptor[5] and vascular endothelial growth factor[6] in head and neck cancers, HER2[7] in lung metastases, HER1[8] in Her1-overexpressing intraabdominal cancers and CA19-9[9] in pancreatic cancer have all been clearly detected, and the use of some of these fluorophore-conjugated antibodies has improved the rate of tumor resection at surgery.

Carcinoembryonic antigen (CEA), a 180-kDa glycosylated protein produced by various tumors, is widely used as a clinical marker for many different types of human cancer, such as gastric, colorectal, lung, liver, pancreatic, breast and ovarian cancer.[10–12] The use of indocyanine green-conjugated anti-CEA antibody for imaging of human gastric cancer cells has been described previously, but only in an *in vitro* context.[13] Anti-CEA antibody conjugated to another near infrared (NIR) fluorescent cyanine dye, DY-676, has been tested *in vivo*.[14]

Although these fluorescent probes are promising, many previous studies could not completely eliminate problems related to background signals from intrinsic fluorophores, which may reduce the sensitivity and specificity of cancer detection. Furthermore, only a few previous studies using fluorophore-conjugated antibodies were able to achieve sub-cellular resolution. Such fine-scale detection could contribute to the improvement of prognosis of cancer patients by identifying micro-lesions in the early phases of primary and metastatic cancers.

Two-photon excitation microscopy has been widely used to analyze various phenomena in living animals.[15,16] Because longer wavelengths are used for two-photon excitation of fluorophores than for conventional methods of fluorescence imaging, this technique has many advantages, including better penetration depth, higher signal-to-background ratio and reduced tissue damage. Together, these features enable imaging of deep tissue at high spatiotemporal resolution.

In this study, we performed *in vivo* cancer imaging in mouse models, using a fluorophore-conjugated anti-CEA antibody in two-photon excitation microscopy, to achieve subcellular resolution. In the future, the method we have developed could be applied in clinical settings.

Materials and Methods

Cell lines and establishment of HT1080-GFP-CEA and MKN45-GFP cells. HT1080 human fibrosarcoma cells expressing GFP were established as described previously.[17,18] To establish HT1080-GFP cells expressing CEA (HT1080-GFP-CEA), pcCAG-CEA was constructed by inserting the human CEA cDNA, cloned from mRNA of MKN45, into vector pcCAG, a modified version of vector pcDEF3[19] in which the EF-1α promoter is replaced by the CAG promoter. HT1080-GFP cells were transfected with pcCAG-CEA and selected with 0.8 mg/mL G418 for 7 days, and then cells expressing high levels of CEA were enriched by two rounds of FACS as described below. Control HT1080-GFP cells were also established by transfection with empty pcCAG vector, followed by selection with 0.8 mg/mL G418 for 7 days. MKN45 human gastric cancer cells were obtained from the American Tissue Culture Collection (Manassas, VA, USA). To establish MKN45 cells expressing GFP (MKN45-GFP), we used a lentiviral expression system as described previously.[18,20] HT1080 and HeLa cells were maintained in DMEM containing 10% FBS supplemented with 100 U/mL penicillin G and 100 μg/mL streptomycin, and MKN45 and MKN28 cells were maintained in RPMI1640 medium containing 10% FBS supplemented with 100 U/mL penicillin G and 100 μg/mL streptomycin. All cells were cultured at 37°C in an atmosphere containing 5% CO_2. HeLa and MKN28 cells were used as CEA-negative controls.

Immunoblotting. Cells were lysed with Nonidet P-40 (NP-40) lysis buffer (20 mM Tris-HCl [pH 7.5], 150 mM NaCl, 1% NP-40). Extracted proteins were separated by SDS-PAGE in 10% (w/v) polyacrylamide gels, and then electro-transferred onto polyvinylidene difluoride (PVDF) membranes. Immunoblotting was performed by incubating the membranes with anti-CEA primary antibody (1:1000 dilution, #2383, CEA/CD66e [CB30] mouse mAb [Cell Signaling Technology, Tokyo, Japan]) for 1 h at room temperature, and then with horseradish peroxidase (HRP)-conjugated goat anti-mouse IgG secondary antibody (1:5000 dilution) for 1 h at room temperature. Specific protein bands were visualized by chemiluminescence (ECL Prime Western Blotting Detection System; GE Healthcare Japan, Tokyo, Japan). β-actin, used as an internal control, was detected with a specific antibody (1:2000 dilution, AC-74; Sigma-Aldrich Japan, Tokyo, Japan) in the same manner.

Flow cytometry analysis and FACS analysis. HT1080-GFP-CEA cells and MKN45 cells were suspended in 2 mM EDTA in PBS, and then washed twice with PBS. Immunostaining was performed by incubating the cells with anti-CEA primary antibody (1:200 dilution, #2383; Cell Signaling Technology) for 1 h on ice, and then with Alexa Fluor 647-conjugated secondary antibody (1:2000 dilution, #A-21235, Alexa Fluor 647 Goat Anti-Mouse IgG (H+L); Invitrogen, Tokyo, Japan) for 1 h on ice. Flow cytometry analysis and cell sorting were performed on a BD FACSAria II cell-sorting system (Becton–Dickinson, Tokyo, Japan).

Immunostaining for *in vitro* fluorescence imaging. HT1080-GFP-CEA, HT1080-GFP, and MKN45-GFP cells were cultured on a cover slip and washed once with PBS. The cells were incubated with 4% (w/v) paraformaldehyde (PFA) and washed three times with PBS, followed by incubation with anti-CEA primary antibody (1:200 dilution, #10094, Anti-Human CEA (1B2) Mouse IgG mAb; IBL, Gunma, Japan) overnight at 4°C. The cells were then washed three times with PBS, followed by incubation with Alexa Fluor 594-conjugated secondary antibody (1:2000 dilution, #A-11005, Alexa Fluor 594 Goat Anti-Mouse IgG [H+L] Antibody; Invitrogen) for 30 min at room temperature. Fluorescence images of the cells were captured with a confocal microscope (objective: ×60; excitation wavelengths: 488 and 561 nm; A1R+ confocal microscope system; Nikon, Tokyo, Japan). Image contrast was adjusted by look-up tables (LUTs) in the software of the microscope (NIS-Elements ver. 4.0; Nikon) under the same condition in each image.

Animal models. All animal procedures were approved by the Committee on Animal Experimentation at Ehime University School of Medicine (#05-RE-1-16) and performed in the animal experiment room of Ehime University according to the guidelines proposed by the Science Council of Japan. Female BALB/c *nu/nu* mice (4–8 weeks old) were purchased from Charles River Japan (Kanagawa, Japan). All *in vivo* experiments were performed on anesthetized mice with a ketamine /xylazine cocktail (35–70 mg/kg: 6–12 mg/kg body weight) via i.p. injection. For the s.c. inoculation model, HT1080-GFP-CEA, HT1080-GFP and MKN45-GFP cells were inoculated s.c. into the mice (1×10^6 cells in 100 μL of culture medium). Seven or eight days after the inoculation, the dorsal skin of the mice was surgically opened to observe the tumor mass on the skin flap. For the pre-incubation experiment, MKN45-GFP cells were immunostained prior to inoculation by overnight incubation with anti-CEA primary antibody (1:200 dilution, #10094; IBL) bound to Alexa Fluor 594-conjugated anti-mouse IgG secondary antibody (1:2000 dilution, #Z-25107, Zenon Alexa Fluor 594 Mouse IgG2a Labeling Kit; Invitrogen). Skin flaps were prepared in the mice as described above, followed by inoculation of 0, 10^4, 10^5 or 10^6 cells in 50 μL of 1% agarose into the connective tissue of each skin flap. For the footpad spontaneous metastasis model, 2×10^6

HT1080-GFP-CEA cells in 20 μL of culture medium were injected into right footpads of the mice. Four weeks after the inoculation, mice were laid in the prone position and the legs were fixed, taking care not to stimulate the tumor. A straight incision of 1 cm was then made in the ipsilateral popliteal region.[21] The popliteal lymph node was exposed and subjected to macroscopic/microscopic observation and histological examination.

***In vivo* macroscopic imaging using a fluorescence zoom microscope.** In the s.c. inoculation model and footpad spontaneous metastasis model, tumors were imaged 24 h after injection of Alexa 594-conjugated anti-CEA antibody (10 or 50 μg/body) via the tail vein. For the pre-incubation experiment, images were acquired immediately after inoculation. *In vivo* macroscopic imaging was performed using a fluorescence zoom microscope (MULTIZOOM AZ100; Nikon) with a GFP-HQ filter set (for GFP) and a Texas Red filter set (for Alexa Fluor 594), and an AZ-Plan Apo 0.5× Plan Fluor objective lens (Nikon). All images were collected with a monochrome digital charge-coupled device camera (C9100–13, ImagEM Enhanced; Hamamatsu Photonics, Shizuoka, Japan).

***In vivo* microscopic imaging using a two-photon excited microscope.** After *in vivo* macroscopic imaging, tumors were subjected to *in vivo* microscopic imaging by two-photon excitation microscopy, as follows. The tumor mass on the skin flap was observed by upright microscopic system (Suppl. Fig. S1). Image acquisition was performed by a water-immersion objective lens. Tumors were surrounded by agarose gel and submerged in saline during the observation. Two-photon excited fluorescence imaging and second harmonic generation (SHG) imaging were performed using a multiphoton microscopy system (A1R+MP; Nikon) with a water-immersion objective lens (CFI75 Apo 25xW MP, numerical aperture: 1.1; Nikon) and an excitation laser (wavelengths: 680–950 nm; repetition rate: 80 MHz; pulse width: 70 fs [MaiTai eHP, Spectra-Physics, CA, USA]). An excitation wavelength of 780 or 800 nm was used for the image acquisition. Emission filters were as follows: 629/56 nm band-pass for Alexa Fluor 594, 525/50 nm band-pass for GFP and 492 nm short-pass for SHG. Image acquisition and processing for 3-D rendering were performed using NIS-Elements version 4.0 (Nikon). Image contrast was adjusted by LUTs in the NIS-Elements version 4.0 (Nikon) under the same condition in each image.

Immunofluorescence on tissue sections. In the footpad spontaneous metastasis model, the popliteal lymph node was resected, fixed with 4% (w/v) PFA overnight at 4°C, and embedded in paraffin. Five-micron sections were deparaffinized and subjected to HE staining and immunofluorescence. For immunofluorescence, anti-CEA antibody (1:200 dilution, #10094, IBL) and anti-GFP antibody (1:1000 dilution, #04404-26, anti-GFP [Rat IgG2a] monoclonal [GF090R]; Nacalai Tesque, Tokyo, Japan) were used as primary antibodies. The sections were then washed three times in Tris-buffered saline with Tween 20 (TBS-T; 50 mM Tris-HCl [pH 7.6], 150 mM NaCl, 0.1% Tween 20), followed by incubation at room temperature for 3 h with Alexa Fluor 568-conjugated anti-mouse IgG (1:500 dilution, #A-11004, Alexa Fluor 568 Goat Anti-Mouse IgG [H+L] Antibody; Invitrogen) and Alexa Fluor 488-conjugated anti-mouse IgG (1:500 dilution, #A-11006, Alexa Fluor 488 Goat Anti-Rat IgG (H+L) Antibody; Invitrogen) as the secondary antibodies. Fluorescence and differential interference contrast images of the sections were observed with a wide-field fluorescence microscope (PlanApo 20×/0.75, PlanApo 40×/0.95, ECLIPSE 80i; Nikon).

Results

Establishment of GFP-expressing and carcinoembryonic antigen-expressing human cancer cells and *in vitro* fluorescence imaging. To characterize and evaluate fluorophore-conjugated anti-CEA antibody for macroscopic and microscopic cancer imaging by two-photon excitation microscopy, we first established CEA-expressing HT1080 human fibrosarcoma cells, and then performed immunoblotting analysis to compare expression of CEA protein among the CEA-expressing HT1080 cells (HT1080-GFP-CEA), control HT1080-GFP cells and MKN45 human gastric cancer cells (MKN45-GFP). As shown in Figure 1(a), MKN45-GFP cells expressed abundant endogenous CEA protein; HT1080-GFP-CEA cells expressed a lower level of exogenous CEA protein; and HT1080-GFP, HeLa and MKN28 cells expressed undetectable levels of endogenous CEA protein.

We then performed FACS analysis to investigate the expression of cell-surface CEA protein in HT1080-GFP-CEA and MKN45-GFP cells (Fig. 1b). After two rounds of FACS sorting, the peak of the histogram of HT1080-GFP-CEA (red line) nearly overlapped that of MKN45-GFP (gray line). After only a single round of sorting, HT1080-GFP-CEA (orange line) had a sub-peak near the peak of the histogram of the negative control (blue line). These results indicate that HT1080-GFP-CEA cells express levels of cell-surface CEA protein similar to those of MKN45 cells.

We next tried to visualize cell-surface CEA protein in HT1080-GFP-CEA and MKN45-GFP cells by fluorescence imaging. To this end, we immunostained cells with anti-CEA antibody and observed them by confocal microscopy (Fig. 1c–e). The fluorescence images confirmed comparable *in vitro* expression of CEA protein on the surfaces of MKN45-GFP (Fig. 1c) and HT1080-GFP-CEA cells (Fig. 1d), but not HT1080-GFP cells (Fig. 1e).

To demonstrate the localization of the CEA protein on the CEA-expressing cells, we provide magnified images of the immunostaining in Supplementary Figure S2. CEA protein on the cell surface (i.e. localized on the plasma membrane) was clearly detected in MKN45-GFP cells and HT1080-GFP-CEA cells. Thus, MKN45-GFP and HT1080-GFP-CEA cells express comparable levels of cell-surface CEA protein that can be specifically recognized by the anti-CEA antibody.

***In vivo* fluorescence macroscopic imaging of tumor masses of CEA-expressing human cancer cells using an Alexa Fluor 594-conjugated anti-CEA antibody.** Next, we attempted to visualize tumor masses of HT1080-GFP-CEA and MKN45-GFP cells *in vivo*, using an Alexa Fluor 594-conjugated anti-CEA antibody. HT1080-GFP, HT1080-GFP-CEA, and MKN45-GFP cells were s.c. implanted into immunodeficient nude mice, and then Alexa Fluor 594-conjugated anti-CEA antibody was injected into tail vein 7 days after inoculation. Twenty-four hours after the injection, fluorescence macroscopic (macro-scale) images were acquired using a fluorescence zoom microscope after the skin flap operation (Fig. 2a,b).[22] In the macroscopic images, tumor formation could be confirmed at all the inoculation sites in both the bright field (BF) and GFP images. Although the fluorescence signals in the surrounding tissues were high, tumor masses of CEA-expressing cells (MKN45-GFP and HT1080-GFP-CEA) could be clearly detected in the Alexa Fluor 594 image (Fig. 2c–e). However, the intensity of the Alexa Fluor 594 fluorescence signal in the tumor mass of CEA-negative cells was not significantly different from that in surrounding tissues. These results suggest that Alexa Fluor

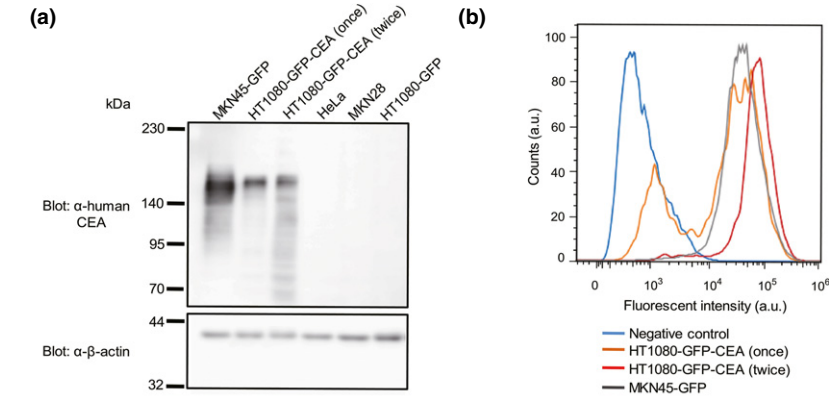

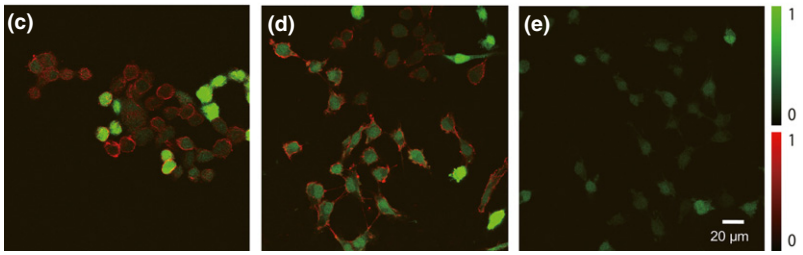

Fig. 1. Establishment of GFP and carcinoembryonic antigen (CEA)-expressing human cancer cells and *in vitro* fluorescence imaging. Comparable expression of CEA protein in HT1080-GFP-CEA and MKN45-GFP cells was confirmed by western blotting, flow cytometry analysis and immunostaining. (a) Western-blotting analysis of CEA expression. HT1080-GFP-CEA cells, subjected to one or two rounds of FACS, were subjected to western blotting alongside MKN45-GFP (CEA-positive) and HeLa, MKN28 and HT1080-GFP (CEA-negative) cells. (b) Flow cytometry analysis of cells expressing CEA. HT1080-GEP-CEA cells were subjected to one or two rounds of FACS, and then analyzed by flow cytometry alongside MKN45-GFP cells. (c–e) Immunostaining of cells to detect CEA. MKN45-GFP (c), HT1080-GFP-CEA (sorted twice) (d) and HT1080-GFP (e) cells were immunostained with anti-CEA primary antibody and Alexa Fluor 594-conjugated anti-mouse IgG secondary antibody (red), and then observed by confocal microscopy (objective: ×60; excitation: 488 nm for GFP and 561 nm for Alexa Fluor 594). Green indicates the GFP fluorescence signal.

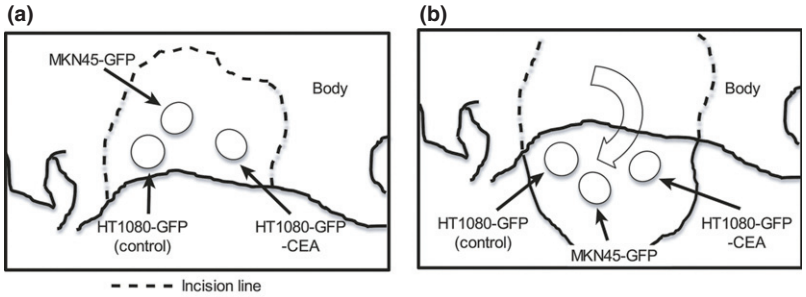

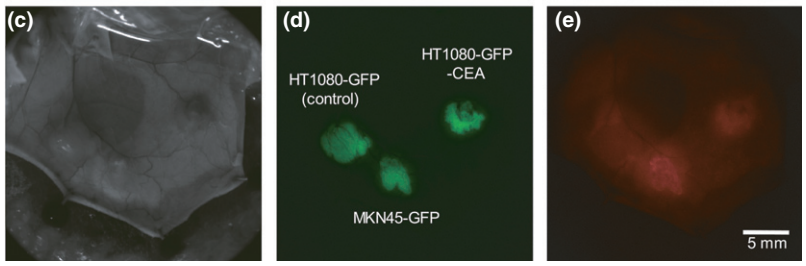

Fig. 2. Inoculation of human cancer cells into immunodeficient mice and *in vivo* macroscopic imaging using a fluorescence zoom microscope. (a) Schema of the sites of inoculation of human cancer cells. The cells were inoculated s.c. into the back skin of nude mice at the rostral–ventral site (HT1080-GFP cells), the caudal–ventral site (HT1080-GFP-CEA cells) or the dorsal site (MKN45-GFP cells). (b) Schema of preparation of skin flaps. Seven or eight days after the inoculation, the inoculation sites were exposed by the skin-flap method. (c–e) *In vivo* macro imaging of tumors. *In vivo* macro imaging of the tumor masses was performed using a fluorescence zoom microscope 24 h after injection of Alexa Fluor 594-conjugated anti-CEA antibody (50 μg/mouse). Exposure times for the GFP and Alexa Fluor 594 fluorescence images were 30 and 100 ms, respectively. These experiments were repeated three times and similar results were obtained.

594-conjugated anti-CEA antibody could specifically visualize tumor masses of CEA-expressing human cancer cells *in vivo*, but the background signals of the surrounding tissues must be distinguished from those of the tumor mass.

***In vivo* microscopic fluorescence imaging of anti-carcinoembryonic antigen-expressing human cancer cells using an Alexa Fluor 594-conjugated anti-carcinoembryonic antigen antibody.** Two-photon excitation microscopy enables collection of fluorescence images in deep tissues at subcellular resolution, as well as capture of nonlinear optical process such as SHG in living tissues.[23] We attempted to visualize the inoculated HT1080-GFP-CEA and MKN45-GFP cells at subcellular resolution, in the same tumors shown in Figure 2, by two-photon excitation microscopy using Alexa Fluor 594-conjugated anti-CEA antibody. GFP signals from three cell lines were detected as shown in the 3-D (Fig. 3a–c) and 2-D reconstructions (Fig. 3d–f) of fluorescence images. In addition, SHG signals were generated from peripheral tissues of the tumors, and to a lesser extent in the tumor stroma. HT1080-GFP-CEA (Fig. 3b, e) and MKN45 cells (Fig. 3c,f), but not HT1080-GFP cells (Fig. 3a,d), could be recognized by the Alexa Fluor 594-conjugated anti-CEA antibody *in vivo*. In the tumor masses of CEA-expressing cells (HT1080-GFP-CEA and MKN45-GFP cells), the Alexa Fluor 594 fluorescence signal was mainly observed on the surfaces of the cancer cells expressing GFP fluorescence in the cytoplasm, but the signal was also detected in the surrounding tissue not containing cancer cells, for example, connective tissue on the tumor surfaces, as depicted by

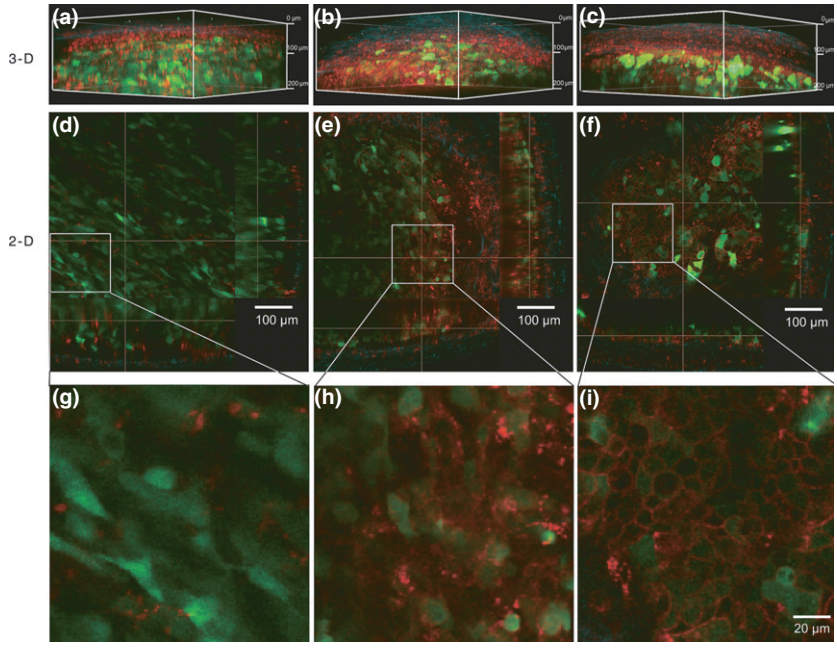

Fig. 3. *In vivo* fluorescence imaging using a two-photon microscope. After the *in vivo* macroscopic imaging as shown in Figure 2(c–e), the same tumors were observed by two-photon excitation microscopy. (a–f) 3-D and 2-D images of HT1080-GFP (a, d), HT1080-GFP-CEA (b, e) and MKN45 (c, f) cells were acquired by two-photon excitation microscopy. Each 2-D image represents an orthogonal view: x-y (center panel), y-z (left panel) and x-z (lower panel). Red, green and blue indicate Alexa Fluor 594 fluorescence, GFP fluorescence and second harmonic generation (SHG), respectively. (g–i) Magnified images of (d–f).

the SHG signal. In CEA-negative cells, the Alexa Fluor 594 fluorescence signal was detected predominantly in surrounding tissue lacking cancer cells.

Moreover, the magnified images of Figure 3(d–f) confirmed that the anti-CEA antibody recognized target proteins localized on the plasma membrane of CEA-expressing cells, resulting in a ring-shaped pattern of fluorescence (Fig. 3g–i). In addition, background signals could be dramatically reduced by decreasing the amount of injected antibody from 50 to 10 μg, while the resultant signals could not be detected by macroscopic imaging (Suppl. Fig. S3 and data not shown). In these two-photon excitation microscopy experiments, the penetration depths in the tumor mass were typically 300–700 μm (data not shown). These results suggest that the combination of Alexa Fluor 594-conjugated anti-CEA antibody and two-photon excitation microscopy enables specific visualization of CEA protein on the cell surface of human cancer cells *in vivo*. Signals from the surfaces of tumor cells could be readily distinguished from those from non-target tissues by their distribution in the tumor mass. Moreover, the characteristic ring-shaped pattern of the signal may be a hallmark of tumor cells expressing CEA on their membrane surfaces. Notably, this feature can only be visualized when subcellular resolution is achieved.

Detection of small numbers of anti-carcinoembryonic antigen-expressing human cancer cells *in vivo* by two-photon excitation microscopy. In order to evaluate the ability of fluorescence-microscopic imaging by two-photon excitation microscopy to detect small numbers of cancer cells labeled with fluorophore-conjugated antibody *in vivo*, MKN45-GFP cells were pre-incubated with Alexa Fluor 594-conjugated anti-CEA antibody overnight, and then 0, 10^4, 10^5 or 10^6 of these cells in 50 μL of 1% agarose were inoculated into the connective tissue of skin flaps (Suppl. Fig. S4). Just after inoculation, macroscopic images were acquired using a fluorescence zoom microscope. As shown in Supplementary Figure S5(a–c), tumor masses of MKN45-GFP cells could be detected by the fluorescence zoom microscope only when 10^6 cells were inoculated. Next, to visualize the same tumors shown in Supplementary Figure S5 at subcellular resolution, we performed two-photon excitation microscopy imaging. 3-D reconstructions (Fig. 4a–d) and the cropped 3-D images (Fig. 4e–h) from two-photon excitation microscopy images revealed that this method allowed MKN45-GFP cells to be detected much more sensitively not only when 10^6 (Fig. 4d,h and Suppl. Fig. S6c), but also 10^4 (Fig. 4b,f and Suppl. Fig. S6a) and 10^5 (Fig. 4c,g and Suppl. Fig. S6b) of the cells were inoculated. In the two-photon experiment, the penetration depths reached within the tumor mass were almost 2 mm. These results suggest that two-photon excitation microscopy using fluorophore-conjugated anti-CEA antibody can achieve deeper and more sensitive cancer cell imaging *in vivo* than conventional imaging using a fluorescence zoom microscope.

***In vivo* fluorescence microscopic imaging of lymph-node metastases by carcinoembryonic antigen-expressing human cancer cells using the Alexa Fluor 594-conjugated anti-carcinoembryonic antigen antibody.** Finally, to further test the usefulness of this combination of two-photon excitation microscopy and fluorophore-conjugated anti-CEA antibody in a more clinically relevant setting, we used this method to detect lymph-node metastases containing HT1080-GFP-CEA cells *in vivo*. In a footpad spontaneous metastasis model using HT1080-GFP-CEA cells, we observed the popliteal lymph node by fluorescence zoom microscopy (Fig. 5a–c) and two-photon excitation microscopy (Fig. 5d–f), respectively. In macroscopic images, lymph-node metastasis could be clearly identified by the GFP fluorescence signal (Fig. 5b); however, contrary to our expectations, the Alexa Fluor 594 signal was not detectable (Fig. 5c). In contrast, in two-photon excitation microscopy, fluorescence of both GFP and Alexa Fluor 594 from the tumor cells in the lymph node could be detected *in vivo* (Fig. 5d–f). We also validated the lymph-node metastasis model by performing immunofluorescence on histological sections (Suppl. Fig. S7). Histologically, metastatic foci occupied small regions inside the lymph nodes, as revealed by HE staining (Suppl. Fig. S7a). Likewise, expression of GFP and CEA protein could be detected in regions of lymph nodes in immunofluorescence images (Suppl. Fig. S7b). These data are consistent with those obtained by two-photon excitation microscopy *in vivo*, which

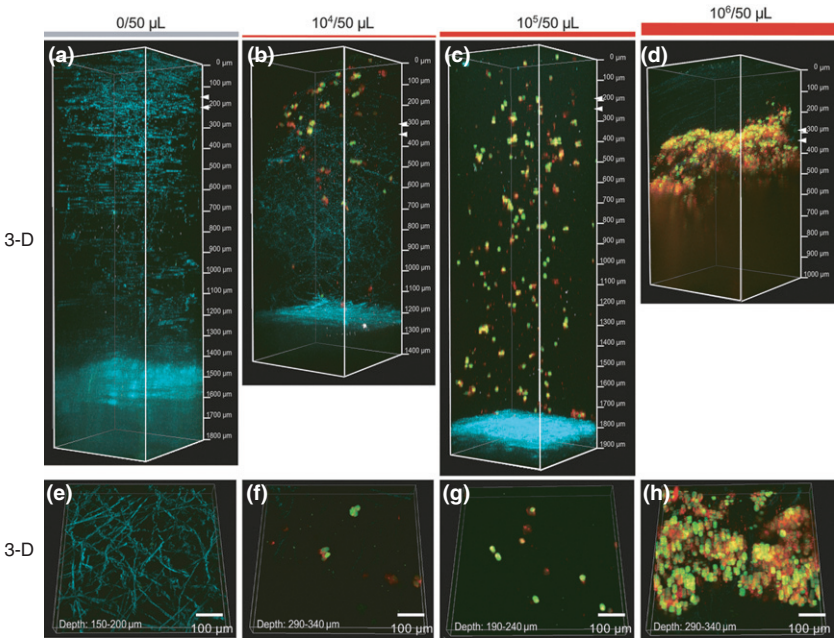

Fig. 4. *In vivo* fluorescence micro imaging of small numbers of cancer cells by two-photon excitation microscopy. *In vivo* micro imaging of the inoculation sites was performed after injection of immunostained MKN45-GFP cells pre-incubated with Alexa Fluor 594-conjugated anti-CEA antibody (see Suppl. Fig. S4). (a–d) 3-D images of sites inoculated with 0 (a and e), 10^4 (b and f), 10^5 (c and g) or 10^6 (d and h) MKN45-GFP cells were acquired by two-photon excitation microscopy. (e–h) Cropped 3-D images of (a–d). The top and bottom of the cropped 3-D images are indicated with two white arrowheads in (a–d). Red, green and blue indicate Alexa Fluor 594 fluorescence, GFP fluorescence and second harmonic generation (SHG), respectively.

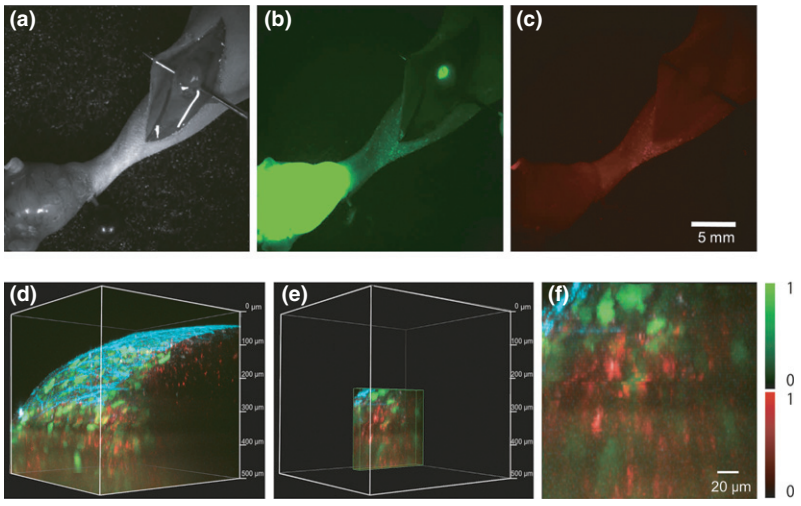

Fig. 5. *In vivo* fluorescence macroscopic and microscopic imaging of lymph-node metastases by a fluorescence zoom microscope and a two-photon excitation microscope. (a–c) A footpad spontaneous metastasis model using HT1080-GFP-CEA cells observed by a fluorescence zoom microscope. The popliteal lymph node was exposed, and multiple images were collected: bright field image (a), GFP (b) and Alexa Fluor 594 (c). Exposure times for the GFP and Alexa Fluor 594 images were 1000 and 3000 ms, respectively. (d–f) Two-photon excitation microscopy of the popliteal lymph node. After *in vivo* macroscopic imaging, the same lymph node was observed using a two-photon excitation microscope. Acquired images are shown as 3-D construction (d), cropped 3-D image of Figure 5d (e) and magnified image of Figure 5e (f), respectively. Red, green and blue indicate Alexa Fluor 594 fluorescence, GFP fluorescence and second harmonic generation (SHG), respectively.

revealed co-localization of GFP and CEA proteins within lymph nodes. These results suggest that use of fluorophore-conjugated anti-CEA antibody in two-photon excitation microscopy can be adapted to preclinical models to detect micrometastasis of tumor cells *in vivo*.

Discussion

Fluorophore-conjugated antibodies against several cell membrane proteins expressed by cancer cells are very useful for specific detection of several cancers in mouse models, as well as in human patients in the clinic.[24,25] In this study, to evaluate macroscopic and microscopic imaging of cancer in mouse models in conjunction with a fluorophore-conjugated antibody, we first established GFP-expressing and CEA-expressing human cancer cell lines, and then demonstrated that cell-surface expression of CEA was comparable in MKN45-GFP cells and FACS-sorted HT1080-GFP-CEA cells. Next, using these cells and control HT1080-GFP cells, we demonstrated that the anti-CEA antibody conjugated to Alexa Fluor 594 could specifically visualize tumor masses of CEA-expressing human cancer cells under the fluorescence zoom microscope. However, the results of macroscopic fluorescence imaging were confounded by high background signals originating from non-target tissues. Of note, fluorescent probes that can be activated only in tumor cells will enable tumor imaging with greater specificity.[26]

The ultimate aim of cancer imaging is visualization of cancers with sufficient specificity and sensitivity to be of clinical usefulness.[3,4] To achieve this, we adopted two-photon excitation microscopy for microscopic imaging of cancer cells using an Alexa Fluor 594-conjugated anti-CEA antibody. Although signals potentially originating from the fluorophore-conjugated antibody were detected in tumor stroma of both CEA-positive and CEA-negative tumors (Fig. 3), signals from the surfaces of tumor cells could be distinguished by their characteristic ring-shaped pattern. These results demonstrated that two-photon excitation microscopy could improve the specificity of tumor imaging by enabling visualization of probes at subcellular resolution.

Another advantage of our technique is better sensitivity. In the experiments depicted in Figure 4, small numbers of cells labeled with a fluorescent probe were inoculated into nude mice at various concentrations. By macroscopic fluorescence imaging, the limit of detection was a 10^6 cells/50 μL. In contrast, much lower concentration (10^4 cells/50 μL) could be visualized at subcellular resolution by two-photon excitation microscopy, confirming the greater sensitivity of this technique. The improved sensitivity was further confirmed in Figure 5, a situation closer to the clinical setting.

Moreover, two-photon excitation microscopy allows intravital imaging with greater penetration and lower toxicity than conventional fluorescence imaging tools such as confocal microscopy.[27] In fact, using two-photon excitation microscopy, we could detect inoculated cancer cells in agarose at penetration depths of nearly 2 mm (Fig. 4), although it must be acknowledged that the areas of observation were filled mostly with agarose. In solid tumor masses, penetration depths were typically several hundred micrometers, which cannot be reached by confocal microscopy.

Considering the advantages of two-photon microscopy described above, we propose that this technique, in combination with fluorescence probes that are safe to use in the human body, could be applied to detection of micro-lesions in clinical settings, for example, carcinoma *in situ*, remaining cancer cells on the resection borders of tumor specimens, and in early phases of lymph-node metastases. At present, these lesions are examined using conventional pathological procedures. Pathological examination has an advantage over fluorescence imaging in that it has no limitation of penetration depth as long as the specimen can be resected. However, fluorescence imaging has the advantage that it enables examination of organs without causing unnecessary damage, which is especially important when the suspicious lesions are not, in fact, malignant.

To facilitate the clinical application of this combination of techniques, it will be necessary to further improve penetration depth and reduce background. One possible solution to this problem would be to use NIR fluorescent substances. Some groups have reported the superiority of NIR fluorophores in regard to signal-to-noise ratio and penetration depth. NIR probes approved for clinical use are yet to be developed.

In conclusion, two-photon excitation microscopy in conjunction with fluorophore-conjugated antibodies has advantages over conventional fluorescence microscopy in regard to specificity, sensitivity and penetration depth. This combination of techniques could be widely adapted to detection of cancer-specific cell-surface molecules, in both cancer research and clinical applications.

Acknowledgments

We thank Dr H. Miyoshi (RIKEN BRC) for lentiviral vectors. We are grateful to H. Ninomiya and N. Miyamoto (Ehime University) for their technical assistance. This study was supported by KAKENHI (Grants-in-Aid for Scientific Research from the Ministry of Education, Culture, Sports, Science and Technology of Japan). T.I. was supported by the Naito Foundation and the Takeda Foundation.

Disclosure Statement

The authors have no conflict of interest to declare.

References

1 Chaffer CL, Weinberg RA. A perspective on cancer cell metastasis. *Science* 2011; **331**: 1559–64.
2 Massoud TF, Gambhir SS. Molecular imaging in living subjects: seeing fundamental biological processes in a new light. *Genes Dev* 2003; **17**: 545–80.
3 Weissleder R, Pittet MJ. Imaging in the era of molecular oncology. *Nature* 2008; **452**: 580–9.
4 Kobayashi H, Longmire MR, Ogawa M, Choyke PL, Kawamoto S. Multiplexed imaging in cancer diagnosis: applications and future advances. *Lancet Oncol* 2010; **11**: 589–95.
5 Withrow KP, Newman JR, Skipper JB *et al.* Assessment of bevacizumab conjugated to Cy5.5 for detection of head and neck cancer xenografts. *Technol Cancer Res Treat* 2008; **7**: 61–6.
6 Kulbersh BD, Duncan RD, Magnuson JS, Skipper JB, Zinn K, Rosenthal EL. Sensitivity and specificity of fluorescent immunoguided neoplasm detection in head and neck cancer xenografts. *Arch Otolaryngol Head Neck Surg* 2007; **133**: 511–5.
7 Koyama Y, Hama Y, Urano Y, Nguyen DM, Choyke PL, Kobayashi H. Spectral fluorescence molecular imaging of lung metastases targeting HER2/neu. *Clin Cancer Res* 2007; **13**: 2936–45.
8 Hama Y, Urano Y, Koyama Y, Choyke PL, Kobayashi H. Activatable fluorescent molecular imaging of peritoneal metastases following pretargeting with a biotinylated monoclonal antibody. *Cancer Res* 2007; **67**: 3809–17.
9 McElroy M, Kaushal S, Luiken GA *et al.* Imaging of primary and metastatic pancreatic cancer using a fluorophore-conjugated anti-CA19-9 antibody for surgical navigation. *World J Surg* 2008; **32**: 1057–66.
10 Cooper EH, Turner R, Steele L, Neville AM, Mackay AM. The contribution of serum enzymes and carcinoembryonic antigen to the early diagnosis of metastatic colorectal cancer. *Br J Cancer* 1975; **31**: 111–7.
11 Wolf B, Thompson J, Von Kleist S. Ultrastructural localization of carcinoembryonic antigen in a continuous human tumour cell line (LS 174 T) in relation to morphometric investigations. *Anticancer Res* 1984; **4**: 213–9.
12 Goldstein MJ, Mitchell EP. Carcinoembryonic antigen in the staging and follow-up of patients with colorectal cancer. *Cancer Invest* 2005; **23**: 338–51.
13 Ito S, Muguruma N, Kusaka Y *et al.* Detection of human gastric cancer in resected specimens using a novel infrared fluorescent anti-human carcinoembryonic antigen antibody with an infrared fluorescence endoscope in vitro. *Endoscopy* 2001; **33**: 849–53.
14 Lisy MR, Goermar A, Thomas C *et al.* In vivo near-infrared fluorescence imaging of carcinoembryonic antigen-expressing tumor cells in mice. *Radiology* 2008; **247**: 779–87.
15 Theer P, Hasan MT, Denk W. Two-photon imaging to a depth of 1000 microm in living brains by use of a Ti:Al_2O_3 regenerative amplifier. *Opt Lett* 2003; **28**: 1022–4.
16 Wyckoff J, Gligorijevic B, Entenberg D, Segall J, Condeelis J. High-resolution multiphoton imaging of tumors in vivo. *Cold Spring Harb Protoc* 2011; **2011**: 1167–84.
17 Hanyu A, Kojima K, Hatake K *et al.* Functional in vivo optical imaging of tumor angiogenesis, growth, and metastasis prevented by administration of anti-human VEGF antibody in xenograft model of human fibrosarcoma HT1080 cells. *Cancer Sci* 2009; **100**: 2085–92.
18 Ehata S, Hanyu A, Fujime M *et al.* Ki26894, a novel transforming growth factor-beta type I receptor kinase inhibitor, inhibits in vitro invasion and in vivo bone metastasis of a human breast cancer cell line. *Cancer Sci* 2007; **98**: 127–33.
19 Goldman LA, Cutrone EC, Kotenko SV, Krause CD, Langer JA. Modifications of vectors pEF-BOS, pcDNA1 and pcDNA3 result in improved convenience and expression. *Biotechniques* 1996; **21**: 1013–5.
20 Katayama K, Wada K, Miyoshi H *et al.* RNA interfering approach for clarifying the PPARgamma pathway using lentiviral vector expressing short hairpin RNA. *FEBS Lett* 2004; **560**: 178–82.
21 Hayashi K, Jiang P, Yamauchi K *et al.* Real-time imaging of tumor-cell shedding and trafficking in lymphatic channels. *Cancer Res* 2007; **67**: 8223–8.
22 Yang M, Baranov E, Wang JW *et al.* Direct external imaging of nascent cancer, tumor progression, angiogenesis, and metastasis on internal organs in the fluorescent orthotopic model. *Proc Natl Acad Sci U S A* 2002; **99**: 3824–9.
23 Chen H, Wang H, Slipchenko MN *et al.* A multimodal platform for nonlinear optical microscopy and microspectroscopy. *Opt Express* 2009; **17**: 1282–90.
24 Hilger I, Leistner Y, Berndt A *et al.* Near-infrared fluorescence imaging of HER-2 protein over-expression in tumour cells. *Eur Radiol* 2004; **14**: 1124–9.
25 Petrovsky A, Schellenberger E, Josephson L, Weissleder R, Bogdanov A Jr. Near-infrared fluorescent imaging of tumor apoptosis. *Cancer Res* 2003; **63**: 1936–42.

26 Urano Y, Asanuma D, Hama Y *et al.* Selective molecular imaging of viable cancer cells with pH-activatable fluorescence probes. *Nat Med* 2009; **15**: 104–9.

27 Centonze VE, White JG. Multiphoton excitation provides optical sections from deeper within scattering specimens than confocal imaging. *Biophys J* 1998; **75**: 2015–24.

Supporting Information

Additional supporting information may be found in the online version of this article:

Fig. S1. Schematic diagram.

Fig. S2. Immunostaining.

Fig. S3. *In vivo* fluorescence micro imaging.

Fig. S4. Experimental flow of pre-incubation assay.

Fig. S5. *In vivo* macro fluorescence imaging.

Fig. S6. *In vivo* fluorescence micro imaging.

Fig. S7. Immunofluorescence and HE staining.